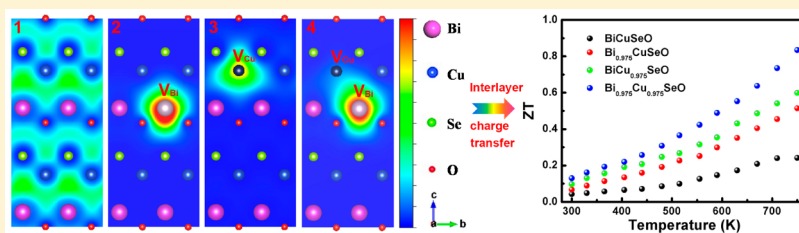


Dual Vacancies: An Effective Strategy Realizing Synergistic Optimization of Thermoelectric Property in BiCuSeO

Zhou Li,[†] Chong Xiao,^{*†} Shaojuan Fan,[‡] Yu Deng,[†] Wenshuai Zhang,[‡] Bangjiao Ye,[‡] and Yi Xie^{*†}

[†]Hefei National Laboratory for Physical Sciences at the Microscale, and Collaborative Innovation Center of Chemistry for Energy Materials, and [‡]State Key Laboratory of Particle Detection and Electronics, University of Science & Technology of China, Hefei, Anhui 230026, People's Republic of China

Supporting Information



ABSTRACT: Vacancy is a very important class of phonon scattering center to reduce thermal conductivity for the development of high efficient thermoelectric materials. However, conventional monovacancy may also act as an electron or hole acceptor, thereby modifying the electrical transport properties and even worsening the thermoelectric performance. This issue urges us to create new types of vacancies that scatter phonons effectively while not deteriorating the electrical transport. Herein, taking BiCuSeO as an example, we first reported the successful synergistic optimization of electrical and thermal parameters through Bi/Cu dual vacancies. As expected, as compared to its pristine and monovacancy samples, these dual vacancies further increase the phonon scattering, which results in an ultra low thermal conductivity of $0.37 \text{ W m}^{-1} \text{ K}^{-1}$ at 750 K. Most importantly, the clear-cut evidence in positron annihilation unambiguously confirms the interlayer charge transfer between these Bi/Cu dual vacancies, which results in the significant increase of electrical conductivity with relatively high Seebeck coefficient. As a result, BiCuSeO with Bi/Cu dual vacancies shows a high ZT value of 0.84 at 750 K, which is superior to that of its native sample and monovacancies-dominant counterparts. These findings undoubtedly elucidate a new strategy and direction for rational design of high performance thermoelectric materials.

INTRODUCTION

Because of their ability to achieve direct and reversible energy conversion between heat and electricity, thermoelectric devices are recognized as a promising candidate for alleviating energy crisis and environmental pollutions.^{1–4} Generally, the conversion efficiency is governed by the dimensionless thermoelectric figure of merit, $ZT = \sigma S^2 T / (\kappa_e + \kappa_l)$, where σ , S , T , κ_e , and κ_l are the electrical conductivity, Seebeck coefficient, absolute temperature, electronic, and lattice thermal conductivity, respectively.^{5,6} However, due to the inverse coupling between the electrical and thermal parameters through inherent electronic structure of materials, the thermoelectric figure of merit, ZT value, is hitherto limited at low values, which strongly hinder the application and commercialization of thermoelectric materials.^{7–9} Therefore, any developed strategies and materials that could compromise or decouple these interrelated parameters should be critical for the breakthrough and ultimate commercialization of thermoelectric technology.^{10–12}

On the road of exploitation in high performance thermoelectric materials, reduction of lattice thermal conductivity has been widely considered to be one of the most effective strategies.^{13–17} It is well-known that the lattice thermal conductivity in solids is governed by phonons, which are the

dissipation of vibrational energy between adjacent atoms through chemical bonding. So, to produce the scattering center for phonons became the key prerequisite in the reduction of lattice thermal conductivity. Because they can break the continuity of chemical bonding by virtue of both missing atom and missing interatomic linkages, vacancies are expected to be efficient scattering sites to reduce thermal conductivity.^{18–23} However, widely investigated monovacancy may also act as electron or hole acceptor, thereby modifying the electronic transport properties and even worsening the thermoelectric performance.²⁴ On the other hand, the amounts as well as distributions of vacancies also influence the thermoelectric properties originating from their contrary contributions to the reduction of lattice thermal conductivity and deterioration of electrical mobility.^{25,26} These issues urge us to create new types of vacancies that scatter phonons effectively while not deteriorating the electrical transport. Most recently, multiple compounds, such as $\text{I}_2\text{-II-IV-VI}_4$,^{27–30} $\text{AgPb}_m\text{SbTe}_{2+m}$,^{31–35} BiCuSeO ,^{36–42} and so on, have attracted the most considerable attention to develop advanced thermo-

Received: February 19, 2015

Published: April 30, 2015

electric materials. As compared to conventional binary compounds, plural kinds of element component in multiple compounds attract our attention, which means we can create new types of vacancies, such as dual or multiple vacancies to overcome the aforementioned issue. In fact, it has been proven that dual vacancies significantly affect the property in other functional materials.^{43–45} For example, it has been found that, in the dual-vacancies dominant NiO,⁴³ carrier concentrations can be modulated by the presence or absence of oxygen defects around nickel defects, which substantively affect its properties. However, this effect has been long neglected in thermoelectric materials. Therefore, it is urgently necessary to develop a new strategy based on the manufacture of dual or multiple vacancies to tackle the essential issue of coupling between electrical and thermal transport properties in thermoelectric materials.

As a typical multiple compound, BiCuSeO shows a unique and tangible structure stacking by alternating insulating $[\text{Bi}_2\text{O}_2]^{2+}$ layers and conductive $[\text{Cu}_2\text{Se}_2]^{2-}$ layers³⁸ along the *c* axis, which provides us an ideal platform to clearly investigate the dual vacancies' effect. Herein, by simultaneously introducing 2.5% Bi and Cu vacancies into the insulating $[\text{Bi}_2\text{O}_2]^{2+}$ layers and conductive $[\text{Cu}_2\text{Se}_2]^{2-}$ layers, respectively, we successfully synergistically optimized the electrical and thermal parameters. As expected, these dual vacancies effectively decrease the lattice thermal conductivity. Most importantly, the clear-cut evidence in positron annihilation unambiguously confirms the interlayer charge transfer between these Bi/Cu dual vacancies, which results in the significant increase of electrical conductivity with a relatively high Seebeck coefficient. As a result, a high ZT value up to 0.84 was achieved in $\text{Bi}_{0.975}\text{Cu}_{0.975}\text{SeO}$ at 750 K, which is nearly 4 times larger than that of the pristine BiCuSeO and superior to the most reported doped counterparts at the same temperature. This charge transfer in heterolayer through dual-vacancies strategy also elucidates a new direction to optimize and design for high performance thermoelectric materials.

EXPERIMENTAL SECTION

Materials. All chemicals were of analytic grade purity purchased from Sinopharm Chemical Reagent Co., Ltd., and used as received without further purification.

Synthesis. Samples with a composition of $\text{Bi}_{1-x}\text{Cu}_{1-y}\text{SeO}$ were synthesized using a one-pot solid-state reaction route. Stoichiometric mixtures of Bi_2O_3 (2N), Bi (4N), Se (AR), and Cu (2.7N) powders were homogenized in agate mortar by hands and sealed in evacuated silica tubes, which were subsequently heated at 573 K for 12 h and then 923 K for 9 h with a 5 K/min heating rate and 2 K/min cooling rate. The obtained bulk materials were then crushed into powders and finely grinded. Finally, the obtained powders were hot-pressed into a disk-shaped sample (pellet) of ϕ 15 mm \times 2.5 mm under the axial compressive stress of 60 MPa in a vacuum at 873 K for 30 min in high-density graphite die. All sample preparation processes, including the weighing of raw materials and grinding of powders, were carried out in air.

Characterization. The structure of these obtained samples was characterized via X-ray diffraction (XRD) pattern, which was recorded on a Rigaku Dmax diffraction system using a Cu $K\alpha$ source ($\lambda = 1.54187$ Å). The field emission scanning electron microscopy (FE-SEM) images were taken on a JEOL JSM-6700F scanning electron microscopy. High-resolution TEM (HRTEM) images and high-angle annular dark-field scanning transmission electron microscopy (HAADF-STEM) images were collected on a spherical aberration-corrected JEOL ARM-200F field-emission transmission electron microscope operating at 200 kV accelerating voltage. Hall coefficient measurements were performed on a Quantum Design Physical

Property Measurement System (PPMS-9) using the van der Pauw method.

Thermoelectric Properties. The resulting discs are extremely brittle and have more than 95% theoretical density, determined from the geometric densities. The samples were well cut and polished with a shiny surface. Rectangular shape samples with typical sizes of 10 mm \times 2 mm \times 2 mm were employed to simultaneously measure electrical conductivity σ and Seebeck coefficient *S* by the standard four-probe methods in a He atmosphere (ULVAC-RIKO ZEM-3). Thermal conductivity κ was calculated using the equation $\kappa = D\rho C_p$ from the thermal diffusivity *D* obtained by a flash diffusivity method (LFA 457, Netzsch) on a round disk sample with diameter of about 10 mm and thickness of 2 mm, and specific heat C_p determined by a differential scanning calorimeter method (DSC Q2000, Netzsch).

Positron Annihilation Spectroscopy. The positron lifetime experiments were carried out with a fast–slow coincidence ORTEC system with a time resolution of about 230 ps full width at half-maximum. A 30 μCi source of ^{22}Na was sandwiched between two identical $\text{Bi}_{1-x}\text{Cu}_{1-y}\text{SeO}$ samples with a total count of two million. The lifetime and the density distribution of a positron in a perfect bulk crystal or that of a positron trapped at a defect were calculated by solving the three-dimensional Kohn–Sham equation with the finite-difference method based on the conventional scheme⁴⁶ and the density functional theory.⁴⁷ To obtain the electron density and the Coulomb potential due to the nuclei and the electron density, several self-consistent calculations for electronic structures were performed with the PBE-GGA approach⁴⁸ or electron–electron exchange–correlations. To obtain the positron lifetimes, the GGA (Generalized Gradient Approximation) form of the enhancement factor proposed by Barbiellini⁴⁹ is chosen.

RESULTS AND DISCUSSION

Prior to transport measurements, the phase purity and crystallinity of the products were investigated by powder X-ray diffraction (XRD) patterns. As shown in Figure 1a, all XRD patterns of the obtained $\text{Bi}_{1-x}\text{Cu}_{1-y}\text{SeO}$ samples could well be indexed to the tetragonal BiCuSeO (*P4/mmm* space group) with lattice parameters of $a = b = 3.93$ Å, $c = 8.93$ Å (JCPDS no. 45-0296). No other peaks were detected, indicating the high purity of these samples. Figure 1b shows an electron diffraction pattern of the $\text{Bi}_{0.975}\text{Cu}_{0.975}\text{SeO}$ sample with selected area aperture of only one grain, which does not show splitting Bragg spots, indicating the single nature of the grain. The two nearest spots with an orientation angle values 90° are fairly consistent with the theoretical values of (001) and (0 $\bar{1}$ 0) planes for tetragonal BiCuSeO; thus the SAED pattern can be easily indexed as the [100] zone axis projection. The high-resolution HAADF-STEM image present in Figure 1c is taken along the [100] zone axis of the $\text{Bi}_{0.975}\text{Cu}_{0.975}\text{SeO}$ sample, which couples both structural and atomic information at the atomic resolution.^{50–52} Taking into account that the contrast in a HAADF image is proportional to $\sim Z^2$ (*Z* being the atomic number), in our $\text{Bi}_{0.975}\text{Cu}_{0.975}\text{SeO}$ sample, Bi atoms are expected to be brighter than both Cu and Se atoms because of their much higher atomic mass. Meanwhile, the O atoms are invisible in the HAADF image, because they are not heavy enough to produce any contrast.⁵² According to the *Z* contrast, the bright and dark stripes in Figure 1c can correspond to $[\text{Bi}_2\text{O}_2]^{2+}$ and $[\text{Cu}_2\text{Se}_2]^{2-}$ layers, respectively. The intensity profiles in Figure 1d and e, recorded along the superimposed white lines in Figure 1c, clearly feature alternate intense and weak peaks due to local contrast variations along the lines. Combined with the superimposed atomic structure in Figure 1c, we can determine the corresponding atoms of each peak accordingly, as labeled in the image. Lattice parameter with $a = b = 3.93$ Å, $c = 8.93$ Å can be easily obtained from the distance

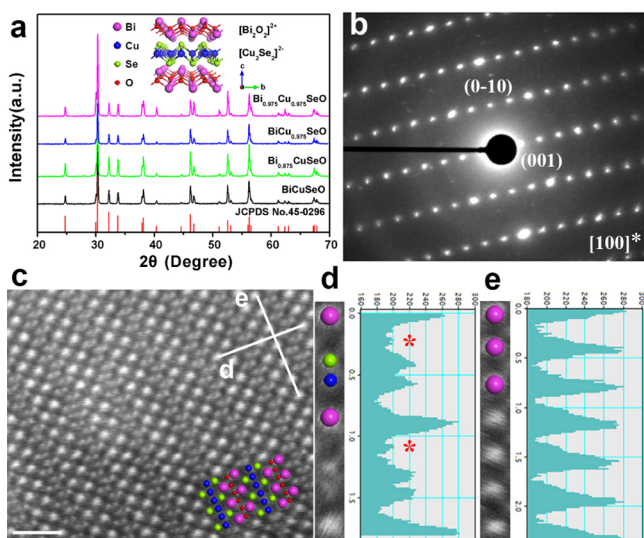


Figure 1. Structure and phase characterization. (a) XRD patterns for $\text{Bi}_{1-x}\text{Cu}_{1-y}\text{SeO}$ samples, the inset displaying the schematic representation of the crystal structure of BiCuSeO along the $[100]$ direction, showing the $[\text{Bi}_2\text{O}_2]^{2+}$ and $[\text{Cu}_2\text{Se}_2]^{2-}$ layers stacking alternately along the c axis. (b) The SAED patterns of the nominal $\text{Bi}_{0.975}\text{Cu}_{0.975}\text{SeO}$ sample, representing a $[100]$ zone axis projection. (c) Experimental obtained $[100]$ HAADF-STEM image of the $\text{Bi}_{0.975}\text{Cu}_{0.975}\text{SeO}$ sample with a superposition of the atomic structure, scale bar, 1 nm, and (d,e) intensity profiles along the superimposed white lines in image (c), corresponding to the $[001]$ axis and $[010]$ axis, respectively. Red asterisks in image (d) point out the existence and specific position of O columns.

between adjacent Bi atoms along the b axis (line e in Figure 1c) and c axis (line d in Figure 1c), respectively, which perfectly match with the theoretical values. It is worth noting that, although O columns are invisible in HAADF images, corroboration of their existence and the specific position can be achieved by the weak foot peaks close to the Bi peaks (Figure 1d, marked by red asterisks).

Because of its nondestructive and selective detection of the negatively charged defects in solid materials with ppm-level sensitivity,^{53–55} positron annihilation spectrometry (PAS) was employed to detailedly study the type and relative concentration of cation vacancies in our samples. As shown in the positron lifetime spectra (Figure 2a) and its derived lifetime parameters (Table 1), the $\text{Bi}_{1-x}\text{Cu}_{1-y}\text{SeO}$ samples yield different lifetime components (range from 3 to 5) due to

composition variation. Pure BiCuSeO has only three lifetime components, among which the predominant shortest component (τ_1 , 175–180 ps) can be ascribed to the bulk lifetime (Table 2), while the two longer life components (τ_4 , 406–418 ps and τ_5 , 1.3–1.9 ns) come from positron annihilation in the large size defects and the interface present in the samples.^{54,55} Bi- and Cu-deficient samples, $\text{Bi}_{0.975}\text{CuSeO}$ and $\text{BiCu}_{0.975}\text{SeO}$, have one more extra lifetime component (τ_2 , around 290 ps for the former, and τ_3 , around 205 ps for the latter), which could be attributed to positron annihilation that trapped at the single isolated Bi (or Cu) vacancies, respectively, according to the theoretically calculated positron lifetime values in Table 2 (as graphically shown in Figure 2b). Naturally, the $\text{Bi}_{0.975}\text{Cu}_{0.975}\text{SeO}$ sample with Bi/Cu dual vacancies shows two more extra lifetime components belong to Bi and Cu vacancies. From the relative intensity of the positron lifetime (Table 1), it is clear that Bi vacancies and Cu vacancies are predominant in the corresponding samples.

Figure 2b represents the projection of the positron density distribution for the (100) plane of pure, Bi-vacancy, Cu-vacancy, and Bi/Cu dual-vacancies samples. It is well-known that the metal vacancies are usually composed by a negatively charged center encircled with positively charged holes. As the positrons are injected into the system, the negatively charged centers will annihilate these positrons. In other words, the positrons usually concentrate at the negatively charged centers, just as shown in Figure 2b-2 and -3, in which the positrons are distributed around the Bi and Cu vacancies in $\text{Bi}_{0.975}\text{CuSeO}$ and $\text{BiCu}_{0.975}\text{SeO}$, respectively. However, in the $\text{Bi}_{0.975}\text{Cu}_{0.975}\text{SeO}$ sample with Bi/Cu dual vacancies (as shown in Figure 2b-4), the positron distribution around Bi vacancy center is more concentrated than that in Figure 2b-2, and the positron distribution around the Cu vacancy center is less concentrated than that in Figure 2b-3. This phenomenon clearly illustrates that positron distribution in the dual-vacancies sample is not a simple superposition by that in monovacancy sample, indicating that a redistribution of carriers should take place in the dual-vacancies system. From Figure 2b-4, we can easily conclude that charge transfers from Bi vacancy centers to Cu vacancy centers, because the positrons are mainly concentrated around Bi vacancies. Taking into account that the holes are the majority charge carriers in p-type $\text{Bi}_{0.975}\text{Cu}_{0.975}\text{SeO}$, this charge transferring from Bi vacancy center ($[\text{Bi}_2\text{O}_2]^{2+}$ insulating layer) to Cu vacancy center ($[\text{Cu}_2\text{Se}_2]^{2-}$ conductive layer) undoubtedly increased carrier concentration (see Figure S1 of the Supporting Information), giving it the highest electrical

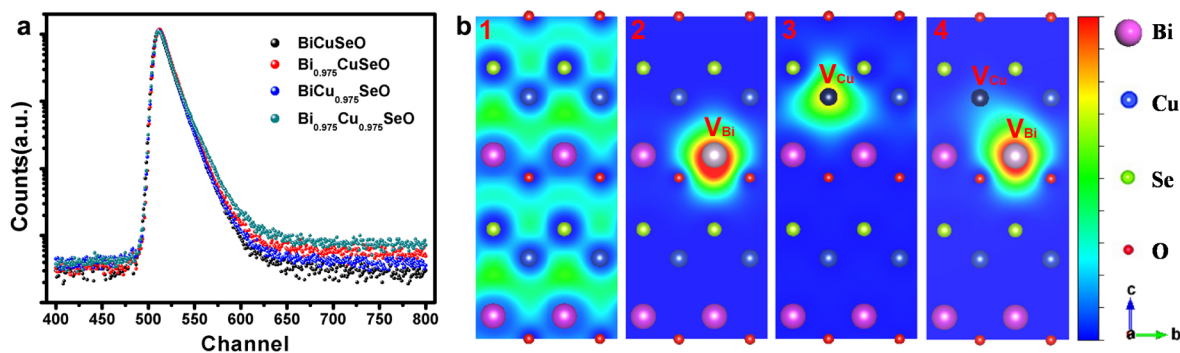


Figure 2. Positron annihilation spectrometry characterization of the $\text{Bi}_{1-x}\text{Cu}_{1-y}\text{SeO}$ samples, showing the interlayer charge transfer in Bi/Cu dual-vacancies $\text{Bi}_{0.975}\text{Cu}_{0.975}\text{SeO}$ sample. (a) Positron lifetime spectrum of $\text{Bi}_{1-x}\text{Cu}_{1-y}\text{SeO}$ samples. (b) Schematic representation of trapped positrons for $\text{Bi}_{1-x}\text{Cu}_{1-y}\text{SeO}$ samples in (100) plane.

Table 1. Positron Lifetime Parameters of $\text{Bi}_{1-x}\text{Cu}_{1-y}\text{SeO}$ Samples

sample	τ_1 (ps)	τ_2 (ps)	τ_3 (ps)	τ_4 (ps)	τ_5 (ns)	I_1 (%)	I_2 (%)	I_3 (%)	I_4 (%)	I_5 (%)
BiCuSeO	178.6			406.2	1.72	79.0			20.7	0.3
$\text{Bi}_{0.975}\text{CuSeO}$	176.7		289.5	417.3	1.90	13.9		69.4	16.5	0.2
$\text{BiCu}_{0.975}\text{SeO}$	179.2	208.1		409.9	1.36	18.4	71.0		10.3	0.3
$\text{Bi}_{0.975}\text{Cu}_{0.975}\text{SeO}$	175.2	205.6	290.2	413.7	1.4	4.1	40.3	45.2	10.2	0.2

Table 2. Calculated Positron Lifetime Values of $\text{Bi}_{1-x}\text{Cu}_{1-y}\text{SeO}$ Samples

	defect		
	bulk	$V_{\text{Bi}}^{\text{'''}}$	$V_{\text{Cu}}^{\text{'}}$
lifetime (ps)	174	289	202

conductivity, which has been proven by the electrical transport properties measurement. The electrical transport properties of our $\text{Bi}_{1-x}\text{Cu}_{1-y}\text{SeO}$ samples were measured, and the results are depicted in Figure 3. Figure 3a shows the temperature dependence of the electrical conductivity for the $\text{Bi}_{1-x}\text{Cu}_{1-y}\text{SeO}$ samples. Pristine BiCuSeO exhibits quite low electrical conductivity values over the entire measuring temperature range. In contrast, Bi- and/or Cu-deficient samples exhibit significantly enhanced electrical conductivity. For example, the conductivity increases from 1300 S m^{-1} (BiCuSeO) to 4700 S m^{-1} ($\text{Bi}_{0.975}\text{Cu}_{0.975}\text{SeO}$) at 750 K.

Figure 3b shows the temperature-dependent Seebeck coefficient for $\text{Bi}_{1-x}\text{Cu}_{1-y}\text{SeO}$. The positive Seebeck coefficient values are indicative of p-type electrical transport behavior of tetragonal BiCuSeO. For pristine BiCuSeO, the Seebeck coefficient is very large, varying from $525 \mu\text{V K}^{-1}$ at 300 K to $382 \mu\text{V K}^{-1}$ at 750 K. The large Seebeck coefficients could be related to the two-dimensional confinement of charge carriers^{7,56} caused by the “natural superlattice” layered structure stacking by alternated insulating $[\text{Bi}_2\text{O}_2]^{2+}$ layers and conductive $[\text{Cu}_2\text{Se}_2]^{2-}$ layers. Upon introducing Bi and/or Cu vacancies, the Seebeck coefficient decreases due to

increased electrical conductivity, but still maintains at $433\text{--}300 \mu\text{V K}^{-1}$ ($\text{Bi}_{0.975}\text{Cu}_{0.975}\text{SeO}$, for example) over the entire measuring temperature range, which is still quite large as compared to most thermoelectric materials.^{2,9,10,57}

Figure 3c shows the thermal conductivity values for $\text{Bi}_{1-x}\text{Cu}_{1-y}\text{SeO}$, with distinct performances between the native and vacancy-modulated samples. The total thermal conductivity for pristine BiCuSeO ($0.86 \text{ W m}^{-1} \text{ K}^{-1}$ at 300 K) is consistent with previous values, and lower than most thermoelectric materials. Such low lattice thermal conductivity may have originated from the weak bonding between layers and low Young's modulus as reported in previous literatures.³⁹ Upon vacancy modulation, thermal conductivities can be further reduced and reach the minimum in the $\text{Bi}_{0.975}\text{Cu}_{0.975}\text{SeO}$ sample with Bi/Cu dual vacancies, for example, $0.63 \text{ W m}^{-1} \text{ K}^{-1}$ at 300 K. Furthermore, thermal conductivity with a negative temperature dependence was maintained over the entire measuring temperature range (see Figure 3c), implying predominant phonon (lattice) contribution.⁵⁸ Normally, the total thermal conductivity is the sum of the electrical and lattice thermal conductivity, that is, $\kappa = \kappa_l + \kappa_e$. According to the Wiedemann–Franz law,⁵⁹ $\kappa_e = L\sigma T$, where L is the Lorenz number obtained from fitting the respective Seebeck coefficient values with an estimate of the reduced chemical potential,⁵⁸ and σ is the electrical conductivity. On the basis of the calculated Lorenz number (as shown in Figure S2 of the Supporting Information), the temperature-dependent κ_e is plotted in Figure 3d. The electrical contribution to the total thermal conductivity is estimated to be less than 0.23% for the pristine BiCuSeO

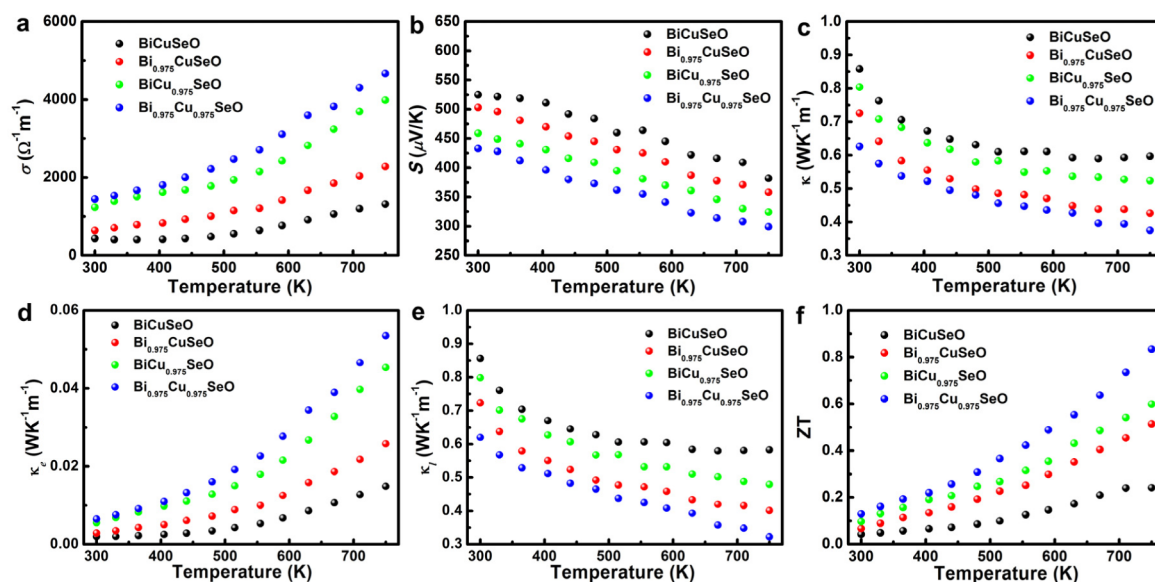


Figure 3. Thermoelectric properties of $\text{Bi}_{1-x}\text{Cu}_{1-y}\text{SeO}$ samples. (a) Temperature-dependent electrical conductivity of $\text{Bi}_{1-x}\text{Cu}_{1-y}\text{SeO}$ samples. (b) Temperature-dependent Seebeck coefficient for $\text{Bi}_{1-x}\text{Cu}_{1-y}\text{SeO}$ samples. (c) Temperature-dependent thermal conductivity (total, κ), (d) electrical thermal conductivity (κ_e), (e) lattice thermal conductivity (κ_l), and (f) dimensionless thermoelectric figure of merit (ZT) for $\text{Bi}_{1-x}\text{Cu}_{1-y}\text{SeO}$ samples.

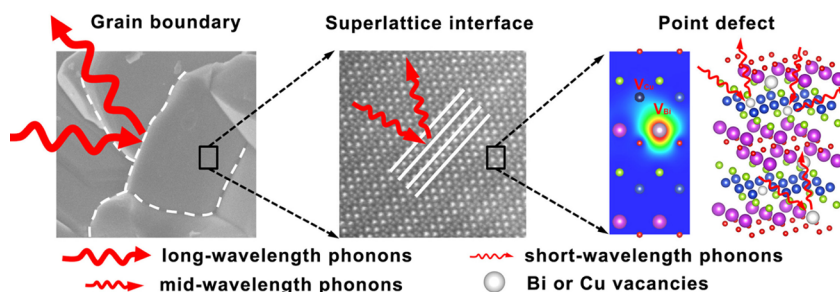


Figure 4. Schematic representation of various phonon scattering mechanism in BiCuSeO with Bi/Cu vacancies. Phonons with different wavelengths are subordinate to different phonon scattering mechanisms. While the grain boundary scattering dominates in the long-wavelength region and the point defects scattering dominates in short-wavelength region, the interfaces between $[\text{Bi}_2\text{O}_2]^{2+}$ and $[\text{Cu}_2\text{Se}_2]^{2-}$ layers can strongly scatter the mid-wavelength phonons, achieving an all-length-scale phonon scattering.

sample and increases maximally to 2.5% at 750 K. These results confirm that the lattice thermal conductivity contribution is predominant for native BiCuSeO, which motivates us to pursue even lower thermal conductivity through reduction of lattice thermal conductivity.

According to the quantum theory, thermal transport is accomplished by energy transfer between heat-carrying phonons through the lattice, which inspires us in that increasing the phonon scattering in solids should be an effective strategy to reduce the lattice thermal conductivity. As aforementioned, vacancies can serve as scattering center to reduce the lattice thermal conductivity by increasing the magnitude and frequency of the scattering event for heat-carrying phonons. Moreover, phonons with different length scales are more likely to be scattered by defects with comparable sizes (see schematic diagram in Figure 4). Thus, in vacancy-modulated $\text{Bi}_{1-x}\text{Cu}_{1-y}\text{SeO}$, while the Bi/Cu vacancies and grain boundaries are favorable for short- and long-wavelength phonon scattering, the superlattice interfaces between adjacent $[\text{Bi}_2\text{O}_2]^{2+}$ and $[\text{Cu}_2\text{Se}_2]^{2-}$ layers can strongly scatter the mid-wavelength phonons, achieving an all-length-scale phonon scattering. Combined with the emerging interlayer charge transfer, phonon scattering by Bi/Cu vacancies can effectively decrease the lattice thermal conductivity with no deterioration of electrical conductivity. As shown in Figure 3e, the lattice thermal conductivity κ_l for vacancy-modulated samples, obtained by directly subtracting κ_e from κ , are obviously lower than the pristine counterpart. Moreover, in dual-vacancies BiCuSeO, by virtue of simultaneous phonon scattering in both insulating $[\text{Bi}_2\text{O}_2]^{2+}$ layers and conductive $[\text{Cu}_2\text{Se}_2]^{2-}$ layers, lattice thermal conductivity was further reduced in dual-vacancies sample as compared to the monovacancy ones, making $\text{Bi}_{0.975}\text{Cu}_{0.975}\text{SeO}$ with Bi/Cu dual vacancies show the minimum lattice thermal conductivity among all of the samples. It is worth noting that because the particle sizes and grain boundaries are identical in $\text{Bi}_{1-x}\text{Cu}_{1-y}\text{SeO}$ with different compositions (see Figures S3, S4 of the Supporting Information for details), the different trends in reduction of thermal conductivity are directly correlated with their vacancy-type differences.

On the basis of the measured electrical and thermal transport properties, the dimensionless thermoelectric figure of merit ZT is calculated as shown in Figure 3f. ZT increases with temperature, with the maximum value 0.84 at 750 K for the dual-vacancies $\text{Bi}_{0.975}\text{Cu}_{0.975}\text{SeO}$ sample, which is superior to its native sample and among the highest values reported for bulk BiCuSeO-based thermoelectric materials when evaluated at the same temperature level (~ 750 K). What is more, the ZT value

holds a “ferocious rally” at higher temperature, and thus we would expect even higher ZT values at higher temperatures. Combined with the aforementioned results, the enhancement is unambiguously correlated to the relative higher electrical conductivity and extremely low thermal conductivity while maintaining a relatively high Seebeck coefficient over the whole temperature range.

CONCLUSION

In summary, we highlight the manufacture of dual vacancies as an effective strategy to synergistically optimize electrical and thermal parameters. Taking BiCuSeO as an example, along with simultaneous introduction of Bi and Cu vacancies into the heterolayer of $[\text{Bi}_2\text{O}_2]^{2+}$ layers and $[\text{Cu}_2\text{Se}_2]^{2-}$ layers, respectively, Bi/Cu dual-vacancies dominant BiCuSeO shows much intensive phonon scattering in the whole system with a result of significant reduction of thermal conductivity as low as $0.37 \text{ W m}^{-1} \text{ K}^{-1}$ at 750 K. Most importantly, the clear-cut evidence from positron annihilation unambiguously elucidates the interlayer charge transfer between these Bi/Cu dual vacancies, which results in the substantial enhancement of electrical with relatively high Seebeck coefficient. In Bi/Cu dual-vacancies $\text{Bi}_{0.975}\text{Cu}_{0.975}\text{SeO}$, induced holes transfer from Bi vacancy center to Cu vacancy center, and participate in the electrical transport process, giving it much higher electrical conductivity of 4700 S m^{-1} at 750 K. As a result, a high ZT value of 0.84 has been obtained at 750 K in the BiCuSeO sample with Bi/Cu dual vacancies, which is superior to that of its native sample as well as monovacancies counterparts. Our dual-vacancies strategy undoubtedly elucidates a new strategy and direction for rational design of high performance thermoelectric materials.

ASSOCIATED CONTENT

Supporting Information

Figures of carrier density (n) and calculated Lorenz number (L) for $\text{Bi}_{1-x}\text{Cu}_{1-y}\text{SeO}$ samples. The Supporting Information is available free of charge on the ACS Publications website at DOI: 10.1021/jacs.5b01863.

AUTHOR INFORMATION

Corresponding Authors

*cxiao@ustc.edu.cn

*yxie@ustc.edu.cn

Notes

The authors declare no competing financial interest.

ACKNOWLEDGMENTS

We thank Prof. Ling Chen, Dr. Hua Lin, and Dr. Hong Chen at the Fujian Institute of Research on the Structure of Matter, Chinese Academy of Sciences, for the thermoelectric property measurements. This work was financially supported by the National Natural Science Foundation of China (21401182, 21331005, and 91422303), the National Basic Research Program of China (2015CB932302), the China Postdoctoral Science Foundation (no. 2014M550347), the Key Laboratory of Neutron Physics (CAEP, 2014DB02), and the Fundamental Research Funds for the Central University (WK 2060190020, WK 2060190027).

REFERENCES

- (1) Bell, L. E. *Science* **2008**, *321*, 1457.
- (2) Poudel, B.; Hao, Q.; Ma, Y.; Minnich, A.; Yu, B.; Dresselhaus, M. S.; Chen, G.; Ren, Z. F. *Science* **2008**, *320*, 634.
- (3) Zhao, L. D.; Lo, S. H.; Zhang, Y. S.; Sun, H.; Tan, G. J.; Uher, C.; Wolverton, C.; Dravid, V. P.; Kanatzidis, M. G. *Nature* **2014**, *508*, 373.
- (4) Xiao, C.; Xu, J.; Li, K.; Feng, J.; Yang, J. L.; Xie, Y. *J. Am. Chem. Soc.* **2012**, *134*, 4287.
- (5) Goldsmid, H. J. In *CRC Handbook of Thermoelectrics*; Rowe, D. M., Ed.; CRC Press: Boca Raton, FL, 1995; p 74.
- (6) Sootsman, J. R.; Chung, D. Y.; Kanatzidis, M. G. *Angew. Chem., Int. Ed.* **2009**, *48*, 8616.
- (7) Xiao, C.; Li, Z.; Li, K.; Huang, P. C.; Xie, Y. *Acc. Chem. Res.* **2014**, *47*, 1287.
- (8) Biswas, K.; He, J. Q.; Blum, I. D.; Wu, C. I.; Hogan, T. P.; Seidman, D. N.; Dravid, V. P.; Kanatzidis, M. G. *Nature* **2012**, *489*, 414.
- (9) Heremans, J. P.; Jovovic, V.; Toberer, E. S.; Saramat, A.; Kurosaki, K.; Charoenphakdee, A.; Yamanaka, S.; Snyder, G. J. *Science* **2008**, *321*, 554.
- (10) Xiao, C.; Xu, J.; Cao, B. X.; Li, K.; Kong, M. G.; Xie, Y. *J. Am. Chem. Soc.* **2012**, *134*, 7971.
- (11) Wu, C. Z.; Feng, F.; Feng, J.; Dai, J.; Peng, L. L.; Zhao, J. Y.; Yang, J. L.; Si, C.; Wu, Z. Y.; Xie, Y. *J. Am. Chem. Soc.* **2011**, *133*, 13798.
- (12) Kim, W.; Zide, J.; Gossard, A.; Klenov, D.; Stemmer, S.; Shakouri, A.; Majumdar, A. *Phys. Rev. Lett.* **2006**, *96*, 045901.
- (13) Voneshen, D. J.; Refson, K.; Borissenko, E.; Krisch, M.; Bosak, A.; Piovano, A.; Cemal, E.; Enderle, M.; Gutmann, M. J.; Hoesch, M.; Roger, M.; Gannon, L.; Boothroyd, A. T.; Uthayakumar, S.; Porter, D. G.; Goff, J. P. *Nat. Mater.* **2013**, *12*, 1028.
- (14) Lee, S.; Esfarjani, K.; Luo, T. F.; Zhou, J. W.; Tian, Z. T.; Chen, G. *Nat. Commun.* **2014**, *5*, 3525.
- (15) Poudeu, P. F. P.; D'Angelo, J.; Kong, H.; Downey, A.; Short, J. L.; Pcionek, R.; Hogan, T. P.; Uher, C.; Kanatzidis, M. G. *J. Am. Chem. Soc.* **2006**, *128*, 14347.
- (16) Schmitt, D. C.; Haldolaarachchige, N.; Xiong, Y.; Young, D. P.; Jin, R.; Chan, J. Y. *J. Am. Chem. Soc.* **2012**, *134*, 5965.
- (17) Kang, J.; Roh, J. W.; Shim, W.; Ham, J.; Noh, J.-S.; Lee, W. *Adv. Mater.* **2011**, *23*, 3414.
- (18) Rhyee, J.-S.; Lee, K. H.; Lee, S. M.; Cho, E.; Kim, S.; Lee, E.; Kwon, Y. S.; Shim, J. H.; Kotliar, G. *Nature* **2009**, *459*, 965.
- (19) Snyder, G. J.; Toberer, E. S. *Nat. Mater.* **2008**, *7*, 105.
- (20) Takabatake, T.; Suekuni, K.; Nakayama, T.; Kaneshita, E. *Rev. Mod. Phys.* **2014**, *86*, 669.
- (21) Heremans, J. P.; Wiendlocha, B.; Chamoire, A. M. *Energy Environ. Sci.* **2012**, *5*, 5510.
- (22) Cook, B. A.; Kramer, M. J.; Herring, J. L.; Han, M.-K.; Chung, D.-Y.; Kanatzidis, M. G. *Adv. Funct. Mater.* **2009**, *19*, 1254.
- (23) Toberer, E. S.; May, A. F.; Snyder, G. J. *J. Chem. Mater.* **2010**, *22*, 624.
- (24) Wan, C. L.; Wang, Y. F.; Wang, N.; Norimatsu, W.; Kusunoki, M.; Koumoto, K. *Sci. Technol. Adv. Mater.* **2010**, *11*, 044306.
- (25) Plirdpring, T.; Kurosaki, K.; Kosuga, A.; Ishimaru, M.; Harnwungmoung, A.; Sugahara, T.; Ohishi, Y.; Muta, H.; Yamanaka, S. *Mater. Trans.* **2012**, *53*, 1212.
- (26) Kim, C.-E.; Kurosaki, K.; Ishimaru, M.; Muta, H.; Yamanaka, S. *J. Electron. Mater.* **2011**, *40*, 999.
- (27) Ibáñez, M.; Zamani, R.; LaLonde, A.; Cadavid, D.; Li, W.; Shavel, A.; Arbiol, J.; Morante, J. R.; Gorsse, S.; Snyder, G. J.; Cabot, A. *J. Am. Chem. Soc.* **2012**, *134*, 4060.
- (28) Zeier, W. G.; LaLonde, A.; Gibbs, Z. M.; Heinrich, C. P.; Panthöfer, M.; Snyder, G. J.; Tremel, W. *J. Am. Chem. Soc.* **2012**, *134*, 7147.
- (29) Liu, M. L.; Chen, I. W.; Huang, F. Q.; Chen, L. D. *Adv. Mater.* **2009**, *21*, 3808.
- (30) Xiao, C.; Li, K.; Zhang, J. J.; Tong, W.; Liu, Y. W.; Li, Z.; Huang, P. C.; Pan, B. C.; Su, H. B.; Xie, Y. *Mater. Horiz.* **2014**, *1*, 81.
- (31) Hsu, K. F.; Loo, S.; Guo, F.; Chen, W.; Dyck, J. S.; Uher, C.; Hogan, T.; Polychroniadis, E. K.; Kanatzidis, M. G. *Science* **2004**, *303*, 818.
- (32) Zhou, M.; Li, J. F.; Kita, T. *J. Am. Chem. Soc.* **2008**, *130*, 4527.
- (33) Karkamkar, A. J.; Kanatzidis, M. G. *J. Am. Chem. Soc.* **2006**, *128*, 6002.
- (34) Barabash, S. V.; Ozolins, V.; Wolverton, C. *Phys. Rev. Lett.* **2008**, *101*, 155704.
- (35) Arachchige, I. U.; Wu, J.; Dravid, V. P.; Kanatzidis, M. G. *Adv. Mater.* **2008**, *20*, 3638.
- (36) Liu, Y.; Zhao, L. D.; Liu, Y. C.; Lan, J. L.; Xu, W.; Li, F.; Zhang, B. P.; Berardan, D.; Dragoë, N.; Lin, Y. H.; Nan, C. W.; Li, J. F.; Zhu, H. M. *J. Am. Chem. Soc.* **2011**, *133*, 20112.
- (37) Lan, J. L.; Liu, Y. C.; Zhan, B.; Lin, Y. H.; Zhang, B. P.; Yuan, X.; Zhang, W. Q.; Xu, W.; Nan, C. W. *Adv. Mater.* **2013**, *25*, 5086.
- (38) Zhao, L. D.; He, J. Q.; Berardan, D.; Lin, Y. H.; Li, J. F.; Nan, C. W.; Dragoë, N. *Energy Environ. Sci.* **2014**, *7*, 2900.
- (39) Pei, Y. L.; He, J. Q.; Li, J. F.; Li, F.; Liu, Q. J.; Pan, W.; Barreateau, C.; Berardan, D.; Dragoë, N.; Zhao, L. D. *NPG Asia Mater.* **2013**, *5*, e47.
- (40) Li, J.; Sui, J. H.; Pei, Y. L.; Barreateau, C.; Berardan, D.; Dragoë, N.; Cai, W.; He, J. Q.; Zhao, L. D. *Energy Environ. Sci.* **2012**, *5*, 8543.
- (41) Sui, J. H.; Li, J.; He, J. Q.; Pei, Y. L.; Berardan, D.; Wu, H. J.; Dragoë, N.; Cai, W.; Zhao, L. D. *Energy Environ. Sci.* **2013**, *6*, 2916.
- (42) Pei, Y. L.; Wu, H. J.; Wu, D.; Zheng, F. S.; He, J. Q. *J. Am. Chem. Soc.* **2014**, *136*, 13902.
- (43) Oka, K.; Yanagida, T.; Nagashima, K.; Kanai, M.; Xu, B.; Park, B. H.; Katayama-Yoshida, H.; Kawai, T. *J. Am. Chem. Soc.* **2012**, *134*, 2535.
- (44) Ural, A.; Griffin, P. B.; Plummer, J. D. *Appl. Phys. Lett.* **1998**, *73*, 1706.
- (45) Choi, S. J.; Kim, K. H.; Yang, W. Y.; Lee, H. I.; Heo, S.; Park, G. S.; Shin, H. J.; Yu, H.; Kim, M.; Cho, S. *Appl. Phys. A: Mater. Sci. Process.* **2013**, *112*, 807.
- (46) Boroński, E.; Nieminen, R. M. *Phys. Rev. B* **1986**, *34*, 3820.
- (47) Kohn, W.; Sham, L. J. *Phys. Rev.* **1965**, *140*, A1133.
- (48) Perdew, J. P.; Burke, K.; Ernzerhof, M. *Phys. Rev. Lett.* **1996**, *77*, 3865.
- (49) Barbiellini, B.; Puska, M. J.; Korhonen, T.; Harju, A.; Nieminen, R. M. *Phys. Rev. B* **1996**, *53*, 16201.
- (50) Zhou, W.; Ross-Medgaarden, E. I.; Knowles, W. V.; Wong, M. S.; Wachs, I. E.; Kiely, C. J. *Nat. Chem.* **2009**, *1*, 722.
- (51) Boulineau, A.; Simonin, L.; Colin, J. F.; Canévet, E.; Daniel, L.; Patou, S. *Chem. Mater.* **2012**, *24*, 3558.
- (52) Mata, M. de la; Magen, C.; Gazquez, J.; Utama, M. I. B.; Heiss, M.; Lopatin, S.; Furtmayr, F.; Fernández-Rojas, C. J.; Peng, B.; Morante, J. R.; Rurali, R.; Eickhoff, M.; Morral, I. A. F.; Xiong, Q. H.; Arbiol, J. *Nano Lett.* **2012**, *12*, 2579.
- (53) Tuomisto, F.; Makkonen, I. *Rev. Mod. Phys.* **2013**, *85*, 1583.
- (54) Xiao, C.; Qin, X. M.; Zhang, J.; An, R.; Xu, J.; Li, K.; Cao, B. X.; Yang, J. L.; Ye, B. J.; Xie, Y. *J. Am. Chem. Soc.* **2012**, *134*, 18460.
- (55) Guan, M. L.; Xiao, C.; Zhang, J.; Fan, S. J.; An, R.; Cheng, Q. M.; Xie, J. F.; Zhou, M.; Ye, B. J.; Xie, Y. *J. Am. Chem. Soc.* **2013**, *135*, 10411.

(56) Ohta, H.; Kim, S. W.; Mune, Y.; Mizoguchi, T.; Nomura, K.; Ohta, S.; Nomura, T.; Nakanishi, Y.; Ikuhara, Y.; Hirano, M.; Hosono, H.; Koumoto, K. *Nat. Mater.* **2007**, *6*, 129.

(57) Wu, H. J.; Zhao, L. D.; Zheng, F. S.; Wu, D.; Pei, Y. L.; Tong, X.; Kanatzidis, M. G.; He, J. Q. *Nat. Commun.* **2014**, *5*, 4515.

(58) Zhao, L. D.; Berardan, D.; Pei, Y. L.; Byl, C.; Pinsard-Gaudart, L.; Dragoe, N. *Appl. Phys. Lett.* **2010**, *97*, 092118.

(59) Mahan, G. D.; Bartkowiak, M. *Appl. Phys. Lett.* **1999**, *74*, 953.